Molecular Dynamics Simulation of Solvated Protein at High Pressure†

Douglas B. Kitchen,‡ Lynne H. Reed, and Ronald M. Levy*

Department of Chemistry, Rutgers University, New Brunswick, New Jersey 08903

Received May 4, 1992; Revised Manuscript Received July 24, 1992

ABSTRACT: We have completed a molecular dynamics simulation of protein (bovine pancreatic trypsin inhibitor, BPTI) in solution at high pressure (10 kbar). The structural and energetic effects of the application of high pressure to solvated protein are analyzed by comparing the results of the high-pressure simulation with a corresponding simulation at low pressure. The volume of the simulation cell containing one protein molecule plus 2943 water molecules decreases by 24.7% at high pressure. This corresponds to a compressibility for the protein solution of $\beta = 1.8 \times 10^{-2}$ kbar^{-1}. The compressibility of the protein is estimated to be about one-tenth that of bulk water, while the protein hydration layer water is found to have a greater compressibility as compared to the bulk, especially for water associated with hydrophobic groups. The radius of gyration of BPTI decreases by 2% and there is a one third decrease in the protein backbone atomic fluctuations at high pressure. We have analyzed pressure effects on the hydration energy of the protein. The total hydration energy is slightly (4%) more favorable at high pressure even though the surface accessibility of the protein has decreased by a corresponding amount. Large pressure-induced changes in the structure of the hydration shell are observed. Overall, the solvation shell waters appear more ordered at high pressure; the pressure-induced ordering is greatest for nonpolar surface groups. We do not observe evidence of pressure-induced unfolding of the protein over the 100-ps duration of the high-pressure simulation. This is consistent with the results of high-pressure optical experiments on BPTI. The utility of pressure studies for probing solvent effects on protein stability is discussed.

Pressure-dependent studies of the optical spectra of dissolved solutes have provided a wealth of information about molecular aspects of solute–solvent interactions (van Eldik & Jonas, 1987). In biophysical chemistry, pressure has long been used as an environmental variable to probe the interactions of proteins with ligands and to study conformational equilibria, protein dynamics, and other properties of the native state of proteins (Weber & Drickamer, 1983; Heremans, 1982; Jannasch et al., 1987; Frauenfelder et al., 1990). Studies of pressure effects on proteins have also revealed that proteins unfold at high pressures (Zipp & Kauzmann, 1973; Li et al., 1976; Carrier et al., 1990). Pressure-induced unfolding has been detected both by optical methods and by hydrogen exchange (Wong, 1988, 1991). Recently, an X-ray crystallographic study of a protein at modestly elevated pressure (1 kbar) has been reported which provides information about the anisotropic response of the protein to applied pressure (Kundrot & Richards, 1987). Pressure studies of proteins have also been used to probe the physical properties of the protein hydration layer (Kundrot & Richards, 1988). We have completed a molecular dynamics simulation of solvated protein, bovine pancreatic trypsin inhibitor (BPTI), in solution at high pressure. The structural and energetic effects of the application of high pressure to solvated protein are analyzed by comparing the results of the high-pressure simulation with a corresponding simulation at low pressure. To our knowledge this is the first report of the molecular dynamics simulation of a protein in solution at variable pressures.

The application of pressure to a protein solution provides a way to perturb the structure of the protein and its interactions with solvent in a continuous and controlled way. It is expected that the application of pressure will reduce the packing defects in a protein which will lead to more compact conformations and perhaps to reduced mobility of the atoms within the protein as well. Molecular dynamics simulations constitute a powerful approach to study the relationship between protein conformation and atomic mobility as has been demonstrated in the many studies at ambient pressures (McCammon & Harvey, 1988). Molecular dynamics simulations can be used to estimate the compressibility of a protein. Compressibilities have been estimated from sound velocity experiments (Gavish, 1983; Gekko & Noguchi 1979) and from a crystal structure analysis (Kundrot & Richards, 1987). The compressibility is of interest because it is a direct measure of volume fluctuations. However, it is not possible in these experiments to extract separately a compressibility for the protein and a compressibility for the hydration layer surrounding the protein. In molecular dynamics simulations, on the other hand, the calculation of quantities corresponding to thermodynamic observables can be partitioned into contributions from protein, hydrating waters, and bulk solvent. This analysis can be helpful in developing procedures to carry out the corresponding partitioning of experimental data. Despite the intense interest in the physical characterization of the hydration shell of proteins, the interpretation of experimental thermodynamic data remains equivocal. Several recent high-resolution experimental X-ray and NMR studies of the structure and dynamics of the protein hydration layer have appeared [see, e.g., Teeter (1991), Finer-Moore et al. (1992), Kossiakoff et al. (1992), and Otting et al. (1991)].

In this paper we analyze the changes in the structure of BPTI as observed in a 100-ps molecular dynamics simulation at 10 kbar. The changes in the atomic mobility between the low- and high-pressure simulations are reported. The effect of pressure on the protein hydration energy, intramolecular protein hydrogen bonding, and protein–solvent hydrogen bonding are also analyzed. Protein–water pair distribution

† This research was supported by the NIH (Grant GM 30580).

* To whom correspondence should be addressed.

‡ Present address: Medical Research Division, American Cyanamid, Pearl River, NY 10965.

0006-2960/92/0431-10083$03.00/0

Table I: Averages of Thermodynamic Properties[a]

	low-pressure simulation			high-pressure simulation		
	10–50 ps	50–100 ps	10–100 ps	10–50 ps	50–100 ps	10–100 ps
temperature (K)	298.4 (1.5)	298.4 (1.6)	298.4 (1.6)	298.4 (1.5)	298.3 (1.6)	298.4 (1.6)
pressure (bar)	112 (103)	109 (105)	111 (104)	10270 (97)	10278 (111)	10274 (107)
volume (Å^3)	97576 (438)	97691 (356)	97640 (435)	78290 (156)	78347 (107)	78322 (105)
density (g cm^{-3})	1.017 (4)	1.018 (4)	1.018 (4)	1.268 (3)	1.269 (3)	1.269 (3)
total energy[b]	−26940 (86)	−26929 (104)	−26934 (93)	−27936 (78)	−27887 (82)	−27909 (80)
kinetic energy	5771 (28)	5772 (30)	5771 (28)	5771 (28)	5771 (30)	5771 (29)
potential energy	−32711 (90)	−32700 (108)	−32705 (111)	−33707 (81)	−33657 (85)	−33679 (67)
nonbonded energy	−34557 (91)	−34585 (76)	−34573 (78)	−35553 (92)	−35519 (56)	−35534 (216)
protein–protein	−4234 (40)	−4242 (36)	−4238 (72)	−4246 (39)	−4246 (43)	−4246 (41)
protein–water	−2136 (255)	−2235 (108)	−2191 (192)	−2272 (162)	−2321 (138)	−2299 (150)
water–water	−28187 (141)	−28108 (66)	−28144 (104)	−29035 (99)	−28952 (61)	−28989 (104)

[a] Standard deviations are in parentheses. [b] All energies are in kilocalories per mole.

functions are used to analyze some of the structural aspects of the pressure-induced changes in the protein hydration shell.

EXPERIMENTAL PROCEDURES

Molecular dynamics simulations have been performed on BPTI in water at low pressure (1 bar) and high pressure (10 kbar) using the IMPACT computer program (Kitchen et al., 1990). The molecular mechanics parameters used for the protein were those published by Weiner et al. (1986) including all hydrogens explicitly; the SPC water model was used for the solvent (Berendsen et al., 1981). The equations of motion were integrated using Andersen's Rattle algorithm with a time step of between 1 and 2 fs (Andersen, 1983; Kitchen et al., 1990). The equilibrated protein plus water coordinates used in the present simulations of pressure effects were taken from an earlier study of BPTI dynamics (Kitchen et al., 1990). We summarize the procedures used to generate these coordinates. The initial coordinates of the protein (4BPTI, referred to as crystal form I) were obtained from the Brookhaven Protein Data Bank (Deisenhofer & Steigemann, 1975; Wlodawer et al., 1987). The protein was placed at the center of an equilibrated box of water of dimensions 43.2 Å by 46.9 Å by 47.3 Å. The dimensions were chosen to accommodate three layers of water molecules surrounding the protein. Waters with the most repulsive interactions with the protein were removed successively until a density of ~1.0 g/cm^3 was reached for the protein plus solvent. The density of the protein is ~1.3 g/cm^3 (Edsall & McKenzie, 1983). The total number of solvent molecules remaining in the box included 2943 water molecules plus six chloride ions added to neutralize the system. The ions were placed at the positions of the highest electrostatic potential of the protein as described previously (Kitchen et al., 1990). The number of protein atoms is 906 including all hydrogens explicitly. The pressure and temperature of the system were controlled using Berendsen's scaling method (Berendsen et al., 1984). This method simulates the coupling of the temperature and pressure of the system to an external bath; the kinetic energy of the system and the volume are scaled at each step so that the fluctuations in these quantities from their averages relax with a characteristic time which is adjustable. The relaxation time for the temperature scaling was 0.010 ps, while the pressure relaxation time was 0.100 ps. A nonbonded interaction list was regenerated every 10 steps (10 fs) using a 9 Å cutoff. A residue-based cutoff procedure was used for the protein–protein interactions. That is, if the minimum distance between any two atoms in the two residues was less than 9 Å, then the interactions between all atoms in the two residues were calculated. The cutoff procedure used for protein–water interactions was atom-based on the protein and molecule-based on the water; the water–water interaction cutoff was molecule-based. We did not use a smoothing function to taper the nonbonded interactions at the cutoff as such a procedure is not sensible when using a residue-based cutoff criterion for interactions between protein atoms because of the large spatial extent of a residue. While the application of a smoothing function is commonly used to improve the conservation of energy, we obtain significantly improved conservation of energy for the protein in water system without the smoothing function by using Andersen's algorithm to integrate the equations of motion (Andersen, 1983). Also, we note that the use of a smoothing function in simulations of pure water has been found to suppress the dielectric response (Alper & Levy, 1989).

Two molecular dynamics simulations with periodic boundary conditions, each lasting 100 ps, were completed, differing only in the pressure of the system. The target pressure was 1 bar in one and 10 kbar in the other simulation (1 bar = 0.987 atm). These are referred to in the text as the low- and high-pressure simulations, respectively. Each simulation was equilibrated for 10 ps. Statistics were collected during an additional 90 ps of the two simulations. The coordinates and velocities were saved for analysis every 25 fs. Hydration energies were calculated for each atom of the protein (excluding counterions) using the sum of the Lennard–Jones plus electrostatic interactions of all water molecules within 9 Å from the selected protein atom. Hydration energies for residues and for the entire protein were calculated by summing over the hydration energies of individual atoms. The accessible surface area of the protein was calculated using Richard's method (Richards, 1977). A 1.4-Å probe radius was used for all calculations. The percent solvent accessibility of residue X is calculated relative to the corresponding value for the tripeptide Gly-X-Gly in the extended conformation. That is, we report the percent solvent accessibility of each residue relative to the value for that residue in an extended chain. Protein volumes were calculated according to the Connolly method (Connolly, 1985) as implemented in a program kindly provided to us by Jay Ponder using probe radii of 1.4 and 0 Å (i.e., the volume enclosed by the van der Waals surface) (Kundrot et al., 1991). For the analysis of protein–protein hydrogen bonds, the following criterion was used: the proton donor to heavy-atom acceptor distance must be less than 2.5 Å and the hydrogen-bond angle (A—X···X) must be greater than 120°.

The averages for various thermodynamic properties calculated from the two simulations are listed in Table I. The average temperature in each simulation was 298 K. The volume and density of the simulation cell containing the protein plus water were 97 640 Å^3 and 1.02 g/cm^3 for the low-pressure simulation and 78 322 Å^3 and 1.27 g/cm^3 for the high-pressure

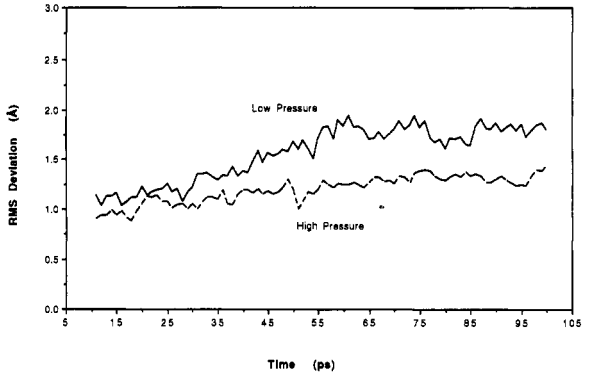

FIGURE 1: Time dependence of the root mean square deviation of the atoms of BPTI from the crystal structure over the course of the simulations. Backbone atom (C, Cα, N, O) root mean squared deviation from the crystal structure form I (solid line, low pressure; dashed line, high pressure).

simulation. The average pressures in the low- and high-pressure simulations were 111 ± 104 and 10 274 ± 107 bar, respectively (1 bar = 0.987 atm). That the average value of the pressure in the low-pressure simulation was 111 bar rather than 1 bar (the target value) is related to the relatively large value of the pressure relaxation time (τ_p = 100 fs) used in these simulations to avoid excessive volume fluctuations (Berendsen et al., 1984). Since the volume change of a water solution on going from 1 bar to 100 bar is very small (less than 1%), the results of the low-pressure simulation at 100 bar should be representative of the behavior of the system close to atmospheric pressure. The total energies, within the standard deviations, are the same during the low- and high-pressure simulations. On the basis of the small fluctuation in the total energy, the lack of drift of the total potential energy, and the comparison of properties calculated over the first and second halves of the simulations (see Table I), as well as an analysis of various structural averages discussed below, we conclude that the simulations are reasonably well equilibrated at both pressures. Comparing the total potential energy of the system at the two pressures, it is slightly more attractive (3%) at the high pressure. This is due to more favorable water–water and water–protein interactions at high pressure, while the protein–protein nonbonded energy is approximately constant at the two pressures. The slight decrease in the water energy with increasing pressure parallels results previously obtained for bulk water (Madura & Pettitt, 1988; Belhadj et al., 1991).

RESULTS

(*i*) *Average Structures.* The rms deviations of the main-chain atoms (residues 3–56) from the crystal structure as a function of time during the two simulations are shown in Figure 1. Overall, the rms deviations of the backbone atoms and the drift during the course of the trajectory are smaller in the high-pressure simulation. At high pressure, the rms deviation between the molecular dynamics structures and the crystal structure (form I) is smaller than ~1.4 Å during the 100-ps simulation. At low pressure, the rms deviation increases from ~1.1 Å at the start of the trajectory to ~1.75 Å during the first 50 ps of the trajectory and then fluctuates about this value for the second half of the trajectory. The average rms deviations by residue are displayed in Figure 2. For the superposition of the two crystal structure coordinate sets, the average deviation per residue is ~0.4 Å. The deviations of the molecular dynamics structures from the crystal structure (form I) at high and low pressure follow similar trends as for

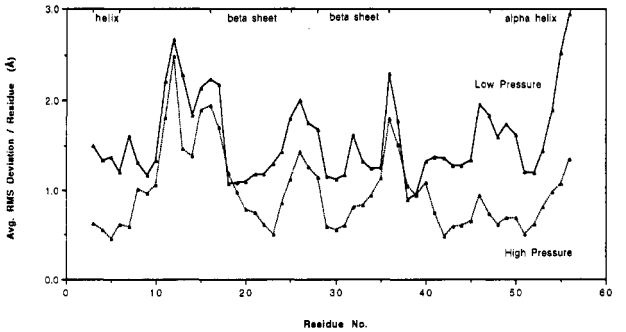

FIGURE 2: Root mean square deviation of the backbone atoms of BPTI from the crystal structure averaged by residue over the 100-ps simulation (solid line, low pressure; dashed line, high pressure).

Table II: Mean Squared Fluctuations of PTI Atomic Positions[a]

	experiment	low pressure	high pressure
all atoms		0.953	0.660
C, Cα, N, O		0.477	0.251
Cα	0.42	0.533	0.345
Cβ	0.46	0.653	0.412
Cγ	0.72	0.783	0.518
Cδ	1.04	0.941	0.618

[a] Mean squared fluctuations were calculated by obtaining the average structure with center of mass translation removed and then calculating the atomic deviation of each structure with rotations removed by taking the best fit of each structure to the average structure. The average atomic squared deviations are the mean squared deviations. All atom averages from the simulations (first row) include hydrogens. The experimental values were calculated from the temperature factors in the 4PTI data set using the relation $(\Delta r)^2 = 3B/8\pi^2$.

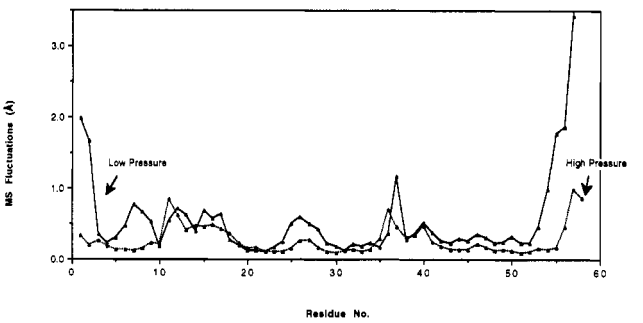

FIGURE 3: Mean squared atomic fluctuations of backbone atoms calculated over the simulation and averaged by residue (solid line, low pressure; dashed line, high pressure).

the deviation between the two crystal forms (Wlodawer et al. 1986). The deviations are largest in the loop regions (rms deviation ~ 1.5 Å) and smallest in the α-helical (rms deviation < 0.4 Å) and β-sheet (rms deviation < 1.0 Å) regions. The rms deviation between low- and high-pressure structures is ~1.06 Å when averaged over the entire trajectory.

(*ii*) *Mean Square Fluctuations.* The mean square fluctuations of the atoms at high pressure have decreased by ~47% compared with the low-pressure values (see Table II and Figure 3). The average mean square fluctuations of the backbone atoms at low pressure is 0.477 ± 0.35 Å^2 and this is reduced to 0.251 ± 0.18 Å^2 at high pressure, while the corresponding values including side-chain atoms are 0.953 and 0.660 Å^2, respectively. Table II lists the average mean square fluctuations for the side-chain carbon atoms proceeding out from the backbone along with the experimental values calculated from the temperature factors of the 4BPTI structure (Wlodawer et al., 1984). The fluctuations at low pressure agree well with the experimental results. The decrease in the side-chain mobility at high pressure, relative to the low-pressure simulation, is of similar magnitude to the pressure effects on the

Table III: Solvation and Solvent Accessibility Statistics

	solvation energy			percent solvent accessibility			
	low pressure	high pressure	percent increase	low pressure	high pressure	percent decrease	crystal structure (form I)
hydrophobic (19)[a]	−133	−129	−3.0	38.1	33.5	13.7	35.1
polar with glycines (24)	−175	−190	8.6	21.0	20.5	2.4	20.2
polar without glycines (18)	−140	−152	8.6	19.0	19.4	−2.1	18.3
glycines (6)	−35	−38	8.6	26.9	23.7	13.5	25.7
negative (5)	−608	−613	0.7	68.6	63.7	7.7	67.2
positive (10)	−1113	−1172	5.3	68.0	63.5	7.1	63.8
all (58)	−2029	−2104	3.7	38.7	35.9	7.8	36.6

Average Surface Area and Volume of PTI[b]

	low pressure	high pressure	form I	form II
surface area (Å^2)	4196 (52)	3897.5 (48)	3990	4082
volume (Å^3) [van der Waals]	6227 (20)	6204 (23)	6299	6213
volume (Å^3) [1.4-Å probe radius]	7453 (37)	7272 (36)	7492	7476

Average Solvation Numbers per Atom[c]

	low pressure	high pressure
carbon, nitrogen, and oxygen (447)	0.826	1.292
carbon (284)	0.495	0.953
nitrogen (84)	1.394	1.844
oxygen (79)	1.410	1.924

[a] The number of each type of residue is given in parentheses. The averages are gathered over all 90 ps. [b] Standard error is given in parentheses. [c] Solvation number is defined as the average number of water molecules within a 3.5-Å spherical shell of an atom. The number of each type of protein atom is given in parentheses.

backbone mobility. Some of the biggest differences between the fluctuations of the atoms at low and high pressure occur at the amino and carboxyl ends of the protein (Figure 3). At low pressure the amino and carboxyl termini of the protein exhibit much greater mobility than the rest of the protein, while at high pressure the fluctuations of the chain ends are comparable in magnitude to the other atoms. There does not appear to be a strong correlation between the magnitude of the mean square fluctuation and the distance from the center of mass at either pressure. The decrease in the atomic mobility at high pressure is distributed throughout the protein. However, at both low and high pressure, the range of the atomic fluctuations increases with distance from the center of mass. Kundrot and Richards recently reported the results of a comparison of the experimental temperature factors for lysozyme obtained from data collected at 1 bar compared with data collected at 1 kbar (Kundrot & Richards, 1988). They observed essentially no decrease in the temperature factors of lysozyme at 1 kbar. In view of the large effects on atomic mobility we observe in the 10-kbar simulation of BPTI, it would be of considerable interest to extend the experimental studies of pressure effects on protein temperature factors to higher pressures and to perform additional simulations at lower pressures.

(*iii*) *Hydration.* The hydration energy of the protein averaged over the full 90 ps is −2191 ± 192 kcal/mol at low pressure and becomes more attractive by 4.7% to −2299 ± 150 kcal/mol at high pressure (Table I). The interaction energy between the protein and the solution has not fully equilibrated at eigher pressure, however; the interaction energy is slightly more favorable in the second half of the simulation as compared with the first half. At low pressure, the average nonbonded energy between the protein and the solution (excluding counterions) is −2136 ± 255 kcal/mol during the first 50 ps and increases to −2235 ± 108 kcal/mol during the second 50 ps. At high pressure, the change in the average solvation energy between the two halves of the trajectory is even smaller; the corresponding values are −2272 ± 162 and −2321 ± 138 kcal/mol, respectively. Although the protein has a slightly more favorable hydration energy at the higher pressure, there is no evidence for pressure-induced protein unfolding during the 100-ps simulation. In fact, at high pressure the protein is more compact. The accessible surface area decreases by 7%, from an average value of 4196 Å^2 at low pressure to 3897 Å^2 at high pressure. The average percent solvent accessibility per residue decreases from 38.7% at low pressure to 35.9% at high pressure.

The changes in hydration energy (excluding the interaction energy with counterions) and surface accessibility with pressure are tabulated by residue type in Table III. For polar and charged residues there is on the average an increase in the hydration energy even though there is often a small decrease in the solvent-accessible surface area as the pressure is increased. Eighty-five percent of the hydration energy of BPTI at low pressure is associated with the hydration of the charged residues and more than two-thirds of the total increase (75 kcal/mol) in the hydration energy of the protein with pressure is attributed to changes in the hydration of the charged residues.

An informative way to analyze pressure effects on the structure of the protein hydration layer is through the analysis of protein–water radial distribution functions. There are two effects which can contribute to pressure-induced changes in the protein–water radial distribution functions: (1) changes in the solvent accessibility due to pressure-induced changes in the average protein structure (i.e., residues may become more or less exposed) and/or (2) changes in the structure of the hydration layer water. Protein–solvent radial distribution functions for representative groups which are solvent-accessible on the protein corresponding to backbone atoms and hydrophobic, polar, and charged side-chain atoms are shown in Figure 4. The corresponding solvation numbers and solvent accessibilities calculated from the simulations are listed in Table IV. In general, the pressure-induced changes in the radial distribution functions for polar and charged atoms on the protein surface are small, since these groups already have a well-structured solvation shell. The number of water molecules in the first hydration shell can be estimated by integrating the radial distribution function out to the first

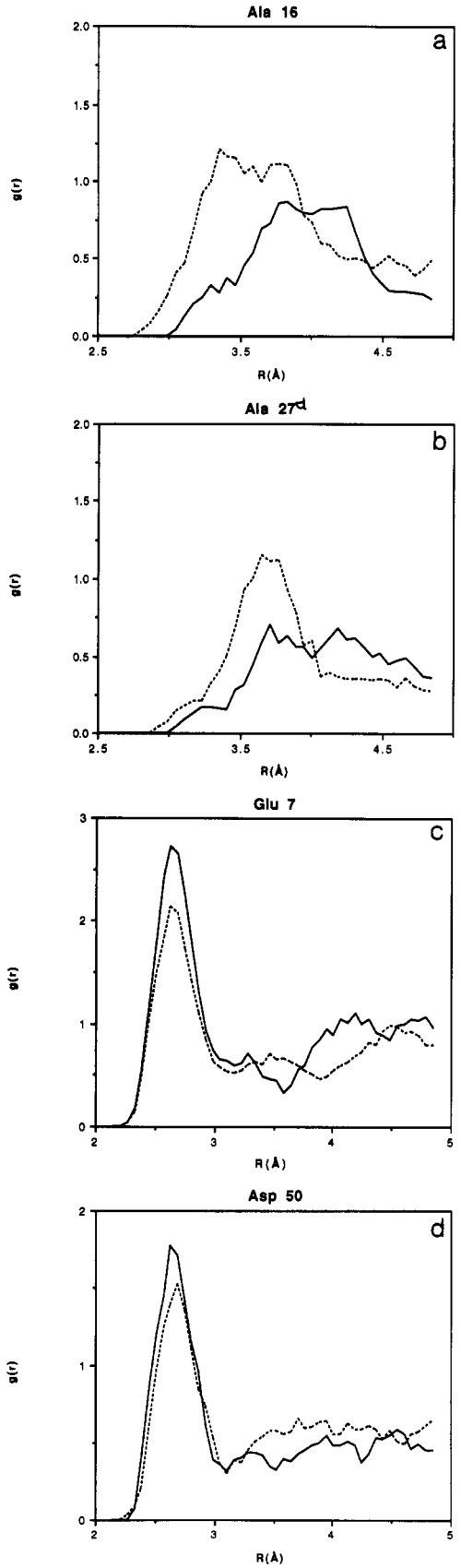

FIGURE 4: Protein to solvent radial distribution functions. Solid lines, low pressure; dashed lines, high pressure. The radial distribution functions are from the solvent (water) oxygen atom to (a) cβ of Ala 16, (b) cβ of Ala 27, (c) Glu 7 Oε (1 and 2), and (d) Asp 50 Oδ (1 and 2).

minimum; the integral must be weighted by the bulk water density, which appears as a normalization factor in the definition of the radial distribution function. Since the bulk water density increases by ~25% at high pressure (10 kbar), the number of hydrating waters (solvation number) surrounding the polar and charged groups increases at high pressure even though the changes in $g(r)$ are small. The average solvation numbers for different atom types at low and high pressure are summarized in Table III and the results for specific residues are listed in Table IV. The number of water molecules within a 3.5-Å spherical shell increases on average from 0.83 waters per protein atom (averaged over all carbon, oxygen, and nitrogen atoms of the protein) at low pressure to 1.29 waters per protein atom at high pressure. The carbon atoms exhibit the largest fractional change in hydration number with pressure (from 0.50 hydrating waters per carbon at low pressure to 0.96 hydrating waters per carbon at high pressure). In contrast, the oxygen and nitrogen atoms, which have similar average hydration numbers, behave differently from the carbon atoms. The oxygens and nitrogens are already hydrated to a greater extent than the carbon atoms at low pressure, and they exhibit a smaller increase in hydration with pressure (from ~1.40 hydrating waters per atom at low pressure to ~1.88 hydrating waters per atom at high pressure).

The largest changes in protein to solvent radial distribution functions with pressure are observed for the hydrophobic groups (see for example $g(r)$ between the methyl group of alanine 27 and water in Figure 4b). From the large increase in the height and width of the first peak of $g(r)$ it is apparent that the application of high pressure has induced the formation of a distinct solvation shell around the hydrophobic groups. A snapshot taken from the low- and high-pressure trajectories (at midway through the simulation) showing the protein backbone structure in ribbon diagram form along with the waters within 4 Å of alanines 16, 25, and 27 appears in Figure 5. The increased solvent density around the alanines is clearly visible in the picture. This kind of effect was observed previously in our simulations of pressure effects on the hydration of a small molecule solute (Belhadj et al., 1991). Even though there is a large change in the solvent structure at the location of the hydrophobic groups on the surface of the protein at high pressure, the change in the hydration energy for these groups is small (Table III). This reflects the fact that hydration energies calculated from the simulations are dominated by electrostatic interactions with the solvent, which are small for the hydrophobic groups. It should be noted that the pressure-induced solvent ordering of the hydration layer can also affect free energies through the entropy of solvation, although pressure-induced entropy changes are not readily calculated from the simulations.

(*iv*) *Hydrogen Bonding.* We have analyzed the pressure effects on the intramolecular (protein–protein) and intermolecular (protein–water) hydrogen bonds. The results are summarized in Tables V and VI; a hydrogen-bond analysis of the two crystal structure forms of BPTI is included for comparison. There is a small increase in the average number of backbone to backbone hydrogen bonds with pressure, from 25.5 observed at low pressure to 27.2 observed at high pressure (Table V). The corresponding numbers calculated from the two crystal structures are 23 (form I) and 21 (form II), respectively (Wlodawer et al., 1987). Of the backbone hydrogen bonds observed in the simulation, there are 17.6 at low pressure and 16.5 at high pressure which are common to one or both of the crystal structures. The average number of backbone to side chain hydrogen bonds increases from 10.5 at low pressure to 13.1 at high pressure. The average number of protein backbone to solvent hydrogen bonds observed in the simulations increases from 45 (low pressure) to 53 (high

Table IV: Solvation Numbers of Selected Protein Atoms

residue	atom	solvation number		percent solvent accessibility			
		low pressure	high pressure	low pressure	high pressure	difference	form I
Ala16	C_β	0.65	2.60	35.7	35.4	−0.3	38.1
Ala25	C_β	0.95	1.70	25.0	18.3	−6.7	37.8
Ala27	C_β	0.30	1.10	48.5	46.6	−1.9	39.5
Ala40	C_β	1.60	0.75	48.7	26.8	−21.9	41.0
Ala48	C_β	1.35	2.75	28.9	22.8	−6.1	26.8
Ala58	C_β	2.20	3.30	125.7	127.2	1.5	134.0
Glu_{49}				66.6	64.9	−1.7	61.5
	$O_{\epsilon 1}$	3.65	4.60				
	$O_{\epsilon 2}$	2.70	3.10				
	$O_{\epsilon 1} + O_{\epsilon 2}$	6.35	7.70				
Asp50				21.3	21.8	0.5	34.0
	$O_{\delta 1}$	2.85	3.30				
	$O_{\delta 2}$	2.80	3.50				
	$O_{\delta 1} + O_{\delta 2}$	5.65	6.80				
Asp3				68.7	72.1	3.4	80.7
	$O_{\delta 1}$	4.15	5.20				
	$O_{\delta 2}$	4.10	4.75				
	$O_{\delta 1} + O_{\delta 2}$	8.25	9.95				
Glu7				38.5	33.9	−4.6	26.0
	$O_{\epsilon 1}$	4.40	4.85				
	$O_{\epsilon 2}$	4.10	4.50				
	$O_{\epsilon 1} + O_{\epsilon 2}$	8.50	9.35				
Arg1				73.3	53.9	−19.4	49.1
	N_ϵ	2.35	0.35				
	$N_{\eta 1}$	3.95	5.90				
	$N_{\eta 2}$	5.35	3.50				
	$N_\epsilon + N_{\eta 1} + N_{\eta 2}$	11.75	9.75				
Arg17				79.5	68.2	−11.3	77.5
	N_ϵ	2.50	3.35				
	$N_{\eta 1}$	4.00	3.75				
	$N_{\eta 2}$	5.05	5.80				
	$N_\epsilon + N_{\eta 1} + N_{\eta 2}$	11.55	12.90				
Tyr21				25.1	24.9	−0.2	25.2
	O_η	2.95	4.90				
Gly37				14.9	16.2	1.3	34.9
	O	1.00	2.45				
Ser47				24.0	22.9	−1.1	24.6
	O_γ	1.85	2.20				
Tyr35				4.6	9.5	4.9	5.7
	O_η	0.70	1.85				
Ala27				48.5	46.6	−1.9	39.5
	O	2.05	3.25				
	N	0.45	0.55				

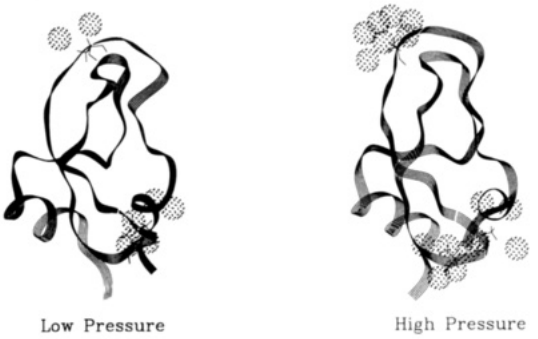

FIGURE 5: Snapshot (at 50 ps) taken from the low- and high-pressure simulations showing the BPTI backbone as a ribbon diagram along with the waters within 4 Å of the cβ of Ala 16, 25, and 27.

Table V: Number of Hydrogen Bonds in the Two Crystal Forms and in the Two Simulations[a]

	crystal	low-pressure simulation	high-pressure simulation
whole protein	33, 31	35.4 ± 2.0	38.0 ± 2.8
total O···HN	23, 21	25.5 ± 2.0	27.2 ± 2.1
O···HN exp list	23, 21	17.6 ± 1.1	16.5 ± 1.2
helix(O···NH)		5.0 ± 0.2	5.1 ± 0.3
O···side chain	3, 3	6.0 ± 1.1	8.5 ± 1.4
N···side chain	4, 4	4.5 ± 0.8	4.6 ± 0.8
side chain···side chain	2, 3	3.4 ± 1.2	3.8 ± 0.9
N*,O*···water		73	80
N,O···water		45	53
C*(side chain)···water		9	28

[a] Hydrogen bonds to water were calculated using radial distribution function maxima less than 3.5 Å. The symbols N*, O*, and C* represent any nitrogen, oxygen, or carbon atom, respectively. N and O represent the backbone atoms only. C* excludes the backbone carbons. A 2.5-Å distance cutoff between hydrogen and acceptor atom and 120° angle between hydrogen, donor, and X was used for the protein–protein hydrogen-bond counts.

pressure). The total number of protein to solvent hydrogen bonds observed in the simulations increases from 73 at low pressure to 80 at high pressure.

In Table VI, heavy-atom donor to acceptor distances for selected protein to solvent hydrogen bonds observed in the BPTI crystal structures are compared with values observed in the low- and high-pressure simulations. While the average hydrogen-bond length between the protein and hydration-layer waters is smaller than values observed in the crystal structure, we do not observe a pressure-induced decrease in the average protein to solvent hydrogen-bond length between the low- and high-pressure simulations. The average donor heavy atom to acceptor distance observed in the crystal structure is 3.07 Å, while in both the low- and high-pressure simulations the average value is 2.88 Å.

Table VI: Comparison of Protein–Water Hydrogen-Bond Distances from the Two Crystal Structure Forms and from the Low- and High-Pressure Simulations[a]

	crystal	low-pressure simulation	high-pressure simulation
form I			
Arg1 N	3.16	2.92	2.92
Asp3 N	2.97		
Ph4 N	3.15		
Tyr21 O_η	3.08	3.00	3.08
Thr32 O_γ	3.00	2.76	3.08
Arg53 N_η	3.20	3.16	3.16
form II			
Tyr10 O_η	3.05	2.68	2.76
Lys15 N_ζ	3.30	3.08	3.00
Ala27 O	2.81	2.84	2.76
Arg39 N_η	3.31	3.16	3.08
Ala40 O	2.92	2.72	2.68
Glu7 O_ϵ[b]	3.35	2.60	2.60
Lys26 O	2.61	2.68	2.68

[a] The water hydrogen-bond distance is the distance corresponding to the radial distribution function maximum between the indicated protein heavy atom and the water oxygen. [b] Alternate position for side chain.

(v) *Protein and Solvent Compression.* Estimates of the compressibility of proteins in the range 5×10^{-3}–2×10^{-2} kbar have been reported (Gekko & Noguchi, 1979; Gavish et al., 1983; Kundrot & Richards, 1988; Saravazyan, 1991). In principle, the compressibility of a protein can be determined from molecular dynamics simulations of solvated protein at two pressures. Such a calculation requires an estimate of the change in the partial specific volume of the protein from the average Cartesian coordinates at the different pressures. Procedures have been developed for calculating the molecular volume of a protein from the Cartesian coordinates, but the conversion of this quantity to a partial molar volume cannot be specified rigorously. We discuss different ways to estimate the compression of the bulk solvent, the solvent hydration layer, and the protein.

We have recently completed simulations from which we were able to calculate the compression of bulk water (the SPC water model) in response to an applied pressure of 10 kbar (Belhadj et al., 1991). The change in density of the SPC water model upon increasing the pressure from 1 bar to 10 kbar was calculated from the simulations to be 25.3%. Using a finite difference–linear response approximation to the compressibility κ_T [$= \ln(\rho_2/\rho_1)/(P_2-P_1)$], the compressibility of the SPC water model is estimated from the simulation to be $\sim 1.8 \times 10^{-2}$ kbar^{-1}. While this is smaller than the experimental value ($\sim 4.5 \times 10^{-2}$ kbar^{-1}), it is expected because of the nonlinear response of water to applied pressure for pressures greater than about 4 kbar (Harr et al., 1984). Using an adaptation (Kundrot et al., 1991) of Connolly's analytical procedure for calculating the volume of a protein, we calculate from the simulations that the average volume of BPTI (using a 1.4-Å probe) is 7453 ± 37 Å^3 at low pressure and decreases by ~2.5% at high pressure to 7272 ± 36 Å^3 (see Table III). On the basis of the calculated change in the protein volume, we estimate that the compressibility of the protein in approximately one-tenth that of bulk water. Subtracting the volume occupied by the protein from the volume of the box, the volume occupied by the solvent is calculated to decrease by 26.9% upon increasing the pressure from 1 bar to 10 kbar. We attribute the (1.6%) increased density of the solvent in the solvated BPTI simulation relative to our results obtained for the high-pressure compression of pure solvent (Belhadj et al. 1991) to the compression properties of the hydration layer. We can very roughly estimate the change in the density of the hydration layer by looking at the pressure-induced change in the number of hydration waters averaged over all protein atoms. The average hydration number is 0.83 at 1 bar and increases to 1.29 at 10 kbar (see Table III). Although it appears as if the density of the hydration layer increases by 60% based on the change in the average hydration number, in this calculation waters are not uniquely partitioned to protein atoms, so that this is an overestimate. We have constructed two different plots of the change in density with pressure of the protein hydration shells to illustrate the effect visually; these are shown in figures 6 and 7 as described below.

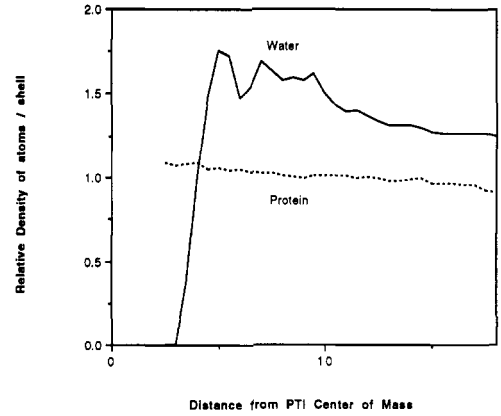

FIGURE 6: Ratio of the solvent densities at high pressure to low pressure in spherical shells surrounding the protein as a function of the distance from the center of mass (solid line), and the corresponding ratio for the protein (dashed line). The values are averages over the 100-ps simulations.

The ratio of the solvent densities at high pressure to low pressure in spherical shells surrounding the protein is plotted as a function of the distance from the center of mass in Figure 6. Even though this coordinate is not orthogonal to the protein surface, and this complicates the interpretation of the figure, one can still see the effects of the increased compressibility of the hydrating waters relative to the compressibility of the bulk waters. The limiting value of 1.25 at large distance corresponds to the change in density of the bulk waters with pressure, while at shorter distances there is a larger increase in density. Notice the appearance of peaks in the relative density which look like first and second hydration shells. However, because the protein is nonspherical there is some averaging of the properties of different hydration shells when the water distribution surrounding the protein is plotted this way. Another way of illustrating the compression of the hydration layer is shown in Figure 7. To construct this figure, each water molecule is tagged in every configuration by the distance of the water oxygen to the nearest protein atom. A histogram is then constructed of the number of water molecules with distance to the closest protein atom specified by an incremental value (2.0–2.2 Å, 2.2–2.4 Å, etc.). Three plots are shown in the figure: (1) the distribution of waters immediately after placing the protein in the box and removing overlapping waters but before equilibration, (2) the distribution of waters around the protein averaged over the low-pressure simulation, and (3) the distribution of waters around the protein averaged over the high-pressure simulation. The formation of a distinct hydration shell around the protein at low pressure with density greater than bulk water, following equilibration of the water around the protein, is clearly seen in the figure. This was also pointed out by Levitt (1988) in his simulation of BPTI in solution. From Figure 7 it can be seen that at high pressure there is a further increase in the density of the hydration layer and the formation of a second hydration shell. In order to better illustrate these effects, we

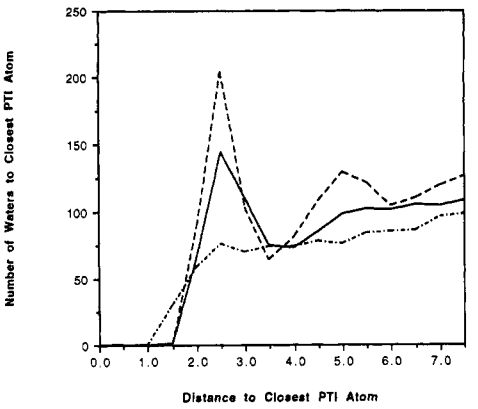

FIGURE 7: Histogram of the number of water molecules as a function of the distance to the closest atom of the protein (dashed line, high pressure; solid line, low pressure; dotted–dashed line, starting point of the simulation before minimization and dynamics).

are working on methods to uniquely partition the space in the simulation cell into regions corresponding to bulk water, first and second hydration layer water, and protein.

We have analyzed pressure effects on distribution functions of the mass density of protein atoms in radial shells about the center of mass. This information is presented in Table VII. Comparing the total mass distribution at low pressure with the distribution at high pressure, the compression of the protein appears as an increase in the mass density toward the center of the protein, with a decrease in mass in each radial shell (2.5-Å thickness) beyond 12.5 Å from the center of mass. The effect of pressure on the distribution of hydrophobic, polar, and charged residues in each radial shell is summarized in Table VII. The compression is not uniform for the different types of residues. There is a larger increase in the density of hydrophobic groups closer to the center of mass, whereas for polar and charged residues, the largest changes in density occur close to the surface.

DISCUSSION

The molecular dynamics simulation of a solvated protein at high pressure has provided a microscopic picture of the effects of high pressure on protein–protein and protein–water interactions. The changes observed in the average protein structure and internal energy upon increasing the pressure to 10 kbar are very small, consistent with estimates of the low compressibility of proteins (Gekko & Noguchi, 1979; Eden et al., 1982; Gavish et al., 1983). This is attributed to both the covalent architecture and the small free volume of the protein. In contrast, there are large changes in the structure of water at the surface of the protein and smaller changes in the average potential energy of interaction between the protein and water. The sensitivity of the hydration shell structure to pressure changes suggests that the use of pressure as a variable in high-resolution experiments can provide new insights into the nature of the hydration forces which stabilize the native protein.

Most of the variable-pressure spectroscopic studies of proteins to date have focused on pressure-induced unfolding. The relative contribution of different physical forces to pressure-induced protein unfolding remains uncertain (Weber & Drickamer, 1983). By Le Chatelier's principle, the high-pressure-denatured state has decreased volume compared with the native state. Electrostriction effects associated with the increased exposure of charged groups in the unfolded state will contribute to the decrease in volume. The large hydration numbers observed in our simulations for charged side chains at low pressure are a manifestation of electrostriction. The electrostriction of solvent hydrating charged groups has been noted previously in simulations of protein hydration (Hagler & Moult, 1978; Levitt & Sharon, 1988; Brooks et al., 1989). On the basis of the results of our simulations at low and high pressure, we conclude that unfolding will to a large extent be driven by increasing the exposed hydrophobic surface area of the protein, since the water hydrating nonpolar groups is more compressible than the bulk. The increased compressibility of the water layer hydrating nonpolar groups and the decreased compressibility of the electrostricted water layer hydrating charged groups, which we have observed in the solvated protein simulations, are also observed in simulations of the hydration of small spherical solutes. For example, the hydration structures calculated from simulations of a small neutral sphere at low and high pressure and a small charged sphere at low and high pressure are shown in Figure 8. The decreased compressibility of the hydration layer due to electrostriction in the charged sphere simulation, and the increased compressibility relative to the bulk, of the hydration waters in the simulation of the neutral sphere solute are clearly seen in the pressure-induced changes in the radial distribution functions of these simple systems.

The compressibility of the hydration layer of model compounds is estimated experimentally from the difference in the compressibilities between dilute solutions containing the solute of interest and pure solvent. Various procedures have been devised to convert the compressibilities of solutions derived from sound velocity measurements to partial molar quantities (Sarvazyan et al., 1992). It should also be noted that different definitions for the partial molar compressibility of a solution are used by different authors [see Edsall and McKenzie (1983)]. The partial molar compressibilities of ionic solutions are almost always negative (Harned & Owen, 1958; Edsall & McKenzie, 1983). Similar behavior has been observed for the zwitterionic amino acids (Millero et al., 1978; Kharakoz, 1991; Sarvazyan et al., 1992). Both positive and negative partial molar compressibilities have been reported for nucleic acids (Buckin 1988). The negative partial molar compressibility of a solution has been interpreted as a decreased compressibility of the hydration sphere of the solute relative to bulk water. For charged solutes this is attributed to electrostriction. However, negative partial molar compressibilities have also been reported for aliphatic amino acids (Kharakoz, 1991) and alcohols (Kauland & Rao, 1979; Edsall & McKenzie, 1983). Perhaps the most notable feature of the partial molar compressibility of hydrophobic solutes is the remarkable sensitivity of the sign of the compressibility to temperature (Edsall & McKenzie, 1983; Kharakoz, 1991; Saravazyan et al. 1992). Near 0 °C the partial molar compressibilities of hydrophobic solutes are qualitatively similar to those of ionic solutes; they reach zero between 20 and 30 °C and become increasingly positive at higher temperatures. Our analysis of compression effects on the hydration layer of different functional groups has been limited to the analysis of changes in the protein–water radial distribution functions with pressure. At the present time, we are not able to compare our results directly with experimental measurements of the partial molar compressibilities of model compounds. In a qualitative sense, however, we expect there to be a positive partial molar compressibility for solutions of hydrophobic solutes at 25 °C on the basis of the changes calculated from the simulations in the solute–solvent radial distribution functions around hydrophobic groups upon the application of pressure. We are planning further analysis of

Table VII: Number of Atoms at Various Distances from Protein Center of Mass

shell distance (Å)	all		hydrophobic		charged		side chain		polar	
	low	high	low	high	low	high	low	high	low	high
2.5	6.70	7.15	3.70	5.375	0.00	0.00	1.80	1.925	3.00	1.775
5.0	51.575	56.025	28.025	31.375	0.475	0.625	19.075	20.90	23.075	24.025
7.5	122.55	127.875	39.15	44.075	24.025	28.075	43.675	40.275	59.375	55.725
10.0	229.65	231.475	65.925	66.725	52.275	50.475	77.85	81.15	111.45	114.275
12.5	231.25	234.725	123.275	114.70	59.00	69.50	68.90	70.95	48.975	50.525
15.0	160.10	154.75	61.80	59.95	82.225	85.175	48.475	48.275	16.075	9.625
17.5	67.25	63.725	22.475	22.925	38.725	28.80	20.525	18.725	6.050	12.00
20.0	31.325	29.425	5.625	4.825	25.70	24.55	12.675	11.70	0.00	0.05
22.5	5.60	0.85	0.025	0.05	5.575	0.80	1.025	0.10	0.00	0.00
25.0	0.00	0.00	0.00	0.00	0.00	0.00	0.00	0.00	0.00	0.00

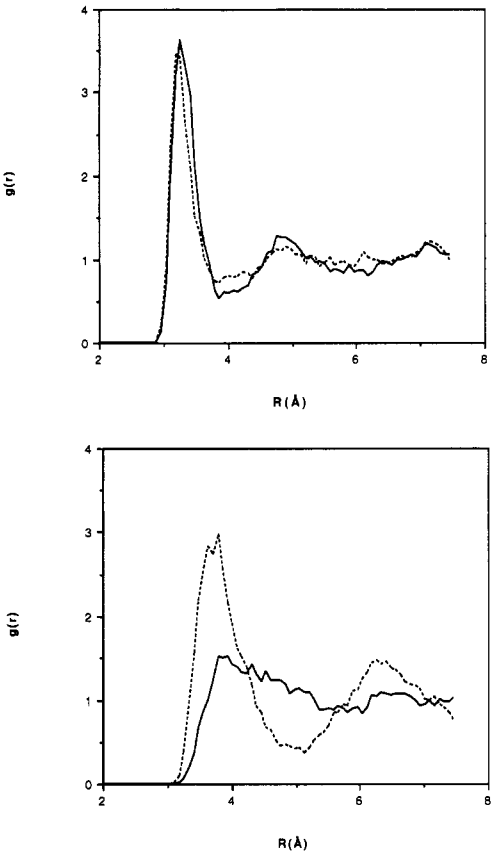

FIGURE 8: Structure of solvent at low and high pressure around a charged sphere (top) and a neutral sphere (bottom). The radial distribution functions are calculated from separate simulations at 1 bar and 10 kbar of a single spherical solute in a box of 216 water molecules. The solute has Lennard–Jones parameters $\sigma/2 = 2.05$ Å and $\epsilon = 0.118$ kcal/mol (these parameters correspond to those of a chloride ion), and the solvent has parameters corresponding to the SPC water model. The radial distribution functions are from the center of the solute to solvent (water) oxygen atom. In the simulation at top, the sphere has a charge −1, and in the simulation at the bottom the solute sphere is neutal. Dashed line, results from the high-pressure simulation; solid line, results from the low-pressure simulation.

the simulations for direct comparison with experimental compressibilities of model compounds.

The fact that the pressure response (compressibility) of waters hydrating different functional groups on the protein surface can be qualitatively grouped into categories according to the chemical type (i.e., charged, polar, and nonpolar; see Tables V and VI and Figure 4) is suggestive of simplified models of protein hydration which associate different thermodynamic states with water surrounding different kinds of residues. In the spirit of models implicit in the simplified hydration scales for proteins that have been proposed, it should be possible to use simulations to evaluate the thermodynamic properties (compressibilities, free energies, etc.) of the waters hydrating different functional groups. We will report on this in a future communication.

The pressure region over which proteins have been observed to denature is variable depending on the protein, but in many cases a single spectral transition is observed with a midpoint in the range 4–8 kbar (Weber & Drickamer, 1983). The changes in fluorescence or absorption usually stabilize at pressures below 10 kbar, but exceptions have also been observed. For example, Visser et al. (1977) found that fluorescence spectral changes under pressure in *Azotobacter* flavodoxin are barely beginning to be observable at 11 kbar. We do not observe a tendency of the backbone of BPTI to unfold in our high-pressure simulations; in fact, the radius of gyration of the protein decreases by 2% in the 10-kbar simulation. It is possible that we do not observe unfolding at high pressure because of the short simulation time. However, the fact that both the intramolecular protein potential energy and the protein–water interaction energy are actually slightly more favorable at the higher pressure suggests that the protein conformations we observe in the high-pressure simulations are not unstable relative to the conformations observed in the low-pressure simulations. The stability of BPTI at high pressure observed in the simulation is consistent with experimental observations based on tyrosine fluorescence.[1] The experimental data provided by Dr. Suzanne Scarlata is illustrated in Figure 9.

While pressure has long been used as an environmental variable in the study of the physical chemistry of proteins, the experiments to date using high-resolution crystallography or NMR spectroscopy have been carried out at only relatively modest pressures (ca. 1 kbar).[2] Kundrot and Richards (1987) report that the compressibility of solvent in lysozyme crystals at 1 kbar is the same as that of the bulk solvent rather than that of an ice or glasslike solid. Our results suggest that the compressibility of waters surrounding hydrophobic groups is very much larger than that of waters hydrating charged groups or even bulk water. Perhaps a cancellation of effects results in a compressibility of the hydration layer averaged over the protein surface which is similar to the bulk; we are investigating this. Kundrot and Richards also report that the number of contacts made between water molecules and apolar protein

[1] After the manuscript was submitted, we were informed by Dr. Suzanne Scarlata, SUNY Stony Brook, of high-pressure fluorescence measurements of BPTI made by Dr. Scarlata while working in the laboratories of Drs. Harry Drickamer and Gregorio Weber at the University of Illinois. The previously unpublished data, reproduced in Figure 9, show that the pressure dependence of the tyrosine fluorescence of BPTI is the same in the presence and absence of quencher up to 10 kbar. This indicates that the application of 10-kbar pressure does not cause major structural changes in the tyrosine domains. See Figure 9 for additional details.

[2] Recently, Dr. Jiri Jonas and co-workers have reported the results of a high-resolution NMR study of the partial unfolding of lysozyme between 1 and 5 kbar (Samarasinghe et al., 1992).

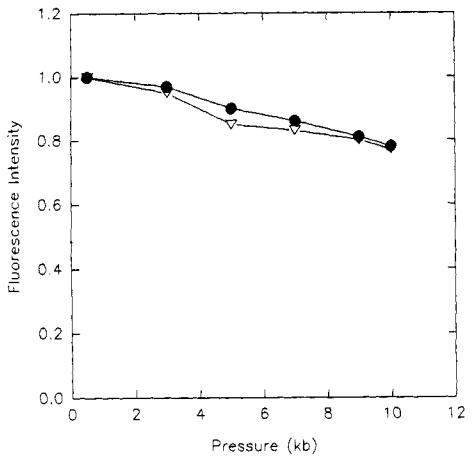

FIGURE 9: Fluorescence intensity of tyrosines from BPTI as a function of pressure in the absence (●) and presence (▽) of quencher. The high-pressure fluorescence measurements were made by Dr. Suzanne Scarlata on the instrumentation in the laboratory of Dr. Harry Drickamer. Excitation was at 270 nm and 0–53 filters were used in the emission. Sodium formate (2 M) was used as a solvent quencher. In the absence of quencher, the emission intensity decreases by about 20% between 0.5 and 10 kbar. This is probably due to changes in the distances between the tyrosines and neighboring quenching groups. The pressure dependence of the fluorescence intensity from BPTI in the presence of quencher is essentially the same as that observed in the absence of quencher.

atoms is essentially unchanged at 1 bar and 1 kbar, whereas our simulations predict that the hydration number of apolar groups should exhibit an increase with increasing pressure. A nonspecific increase in the contacts between water and protein atoms is expected simply on the basis of the increased solvent density. These waters are not necessarily observable in a crystallographic experiment, however. In any case, more crystallographic data over a larger pressure range is needed. Concerning high-resolution NMR studies, an investigation of the rotational motion of the aromatic rings of BPTI has been carried out by Wagner (1980) at variable pressures up to 1.2 kbar. Over the measured range, interpretation of the data for two of the rings (Phe 45 and Tyr 35) using transition-state theory yielded positive activation volumes of about 50 Å^3. Alternative models for the observed positive activation volume have been proposed; the one involves a physical free volume change (Wagner, 1980), while the other focuses on the pressure dependence of the frictional forces on the rings (Karplus & McCammon, 1981). We have not as yet analyzed the rotational dynamics of these residues in our simulations; we do find that average accessibilities and hydration energies of these groups are very similar at both pressures. Simulations of the potentials of mean force for these residues at variable pressure of the kind reported at atmospheric pressure (McCammon & Karplus, 1979; Ghosh & McCammon, 1987) can help to distinguish between the alternative models.

Molecular dynamics simulations have become a routine modeling tool applied to many biophysical problems, but these have been performed under a very narrow set of thermodynamic conditions. The vast majority of protein simulations have been carried out at fixed temperature and constant volume corresponding to ambient conditions. Considerable experimental data exist for calorimetric and spectroscopic probes of the response of proteins to variations in pressure as well as temperature, and information from high-resolution X-ray and NMR studies at variable pressure is beginning to appear. By performing simulations over a larger range of pressures and temperatures, there is the opportunity to obtain greater insight into the microscopic origins of the behavior of proteins under different thermodynamic conditions and, in particular, into the structural and energetic aspects of the protein–solvent interactions which stabilize the native state.

ACKNOWLEDGMENT

We thank Professor Suzanne Scarlata for informing us of her high-pressure studies on BPTI and providing us with the data shown in Figure 9. We thank Professor David Kofke for his work on the constant-pressure algorithm within IMPACT and Professor Jay Ponder for kindly providing us with his program to calculate protein volumes. We acknowledge grants of supercomputer time at the Pittsburgh Supercomputer Center and the National Cancer Institute.

SUPPLEMENTARY MATERIAL AVAILABLE

Four figures showing rms deviation of backbone atoms, mean squared atomic fluctuations of backbone atoms, protein to solvent radial distribution functions, and protein and water densities (4 pages). Ordering information is given on any current masthead page.

REFERENCES

Alper, H., & Levy, R. M. (1989) *J. Chem. Phys. 91*, 1242–1251.
Andersen, H. C. (1983) *J. Comput. Phys. 52*, 24–34.
Belhadj, M., Kitchen, D. B., Krogh-Jespersen, K., & Levy, R. M. (1991) *J. Phys. Chem. 95*, 1082–1089.
Berendsen, H. J. C., Postma, J. P. M., van Gunsteren, W. F., & Hermans, J. (1981) *Intermolecular Forces* (Pullman, B., Ed.) pp 331–334, Reidel, Dordrecht, The Netherlands.
Berendsen, H. J. C., Postma, J. P. M., van Gunsteren, W. F., DiNola, A., & Haak, J. R. (1984) *J. Chem. Phys. 81*, 3684–3689.
Brooks, C. L., Karplus, M., & Pettitt, B. M. (1989) *Proteins: A Theoretical Perspective of Dynamics, Structure, and Thermodynamics*, Advances in Chemical Physics, Vol. LXXI, John Wiley & Sons, New York.
Buckin, V. A. (1988) *Biophys. Chem. 29*, 283–292.
Carrier, D., Mantsch, H., & Wong, P. T. T. (1990) *Biopolymers 29*, 837–844.
Connolly, M. L. (1985) *J. Am. Chem. Soc. 107*, 1118–1123.
Diesenhofer, J., & Steigermann, W. (1975) *Acta Crystallogr. B31*, 238–250.
Eden, D., Mathew, J. B., Rosa, J., & Richards, F. M. (1982) *Proc. Natl. Acad. Sci. U.S.A. 79*, 815–819.
Edsall, J. T., & McKenzie, H. A. (1983) *Adv. Biophys. 16*, 53–183.
Finer-Moore, J. S., Kossiakoff, A. A., Hurley, J. H., Earnest, T., & Stroud, R. M. (1992) *Proteins: Struct., Funct., Genet. 12*, 203–222.
Frauenfelder, H., Alberding, N. A., Ansari, A., Braunstein, D., Cowen, B. R., Hong, M. K., Iben, I. E. T., Johnson, J. B., Luck, S., Marden, M. C., Mourant, J. R., Ormos, P., Reinisch, L., Scholl, R., Schulte, A., Shyamsunder, E., Sorensen, L. B., Steinbach, P. J., Xie, A., Young, R. D., & Yue, K. T. (1990) *J. Phys. Chem. 94*, 1024–1037.
Gavish, B., Gratton, E., & Hardy, C. J. (1983) *Proc. Natl. Acad. Sci. U.S.A. 80*, 750–754.
Gekko, K., & Noguchi, K. (1979) *J. Phys. Chem. 83*, 2706–2714.
Ghosh, I., & McCammon, J. A. (1987) *Biophys. J. 51*, 637–641.
Haar, L., Gallagher, J., & Kell, G. S. (1984) *NBS/NRC Steam Tables*, Hemisphere Press, New York.
Hagler, A. T., & Moult, J. (1978) *Nature 272*, 222–226.
Harned, H. S., & Owen, B. B. (1958) *The Physical Chemistry of Electrolyte Solutions*, 3rd ed., American Chemical Society Monographs, Vol. 13, p 803, Reinhold, New York.
Heremans, K. (1982) *Annu. Rev. Biophys. Bioeng. 11*, 1–54.

Jannasch, H. W., Marquis, R. E., & Zimmerman, A. M., Eds. (1987) *Current Perspectives in High Pressure Biology*, Adenine Press, New York.

Karplus, M., & McCammon, J. A. (1981) *FEBS Lett. 131*, 34–36.

Kauland, M. V., & Rao, K. S. M. (1979) *J. Chem. Soc., Faraday Trans. 1 75*, 2237–2244.

Kharakoz, D. P. (1991) *J. Phys. Chem. 94*, 5634–5642.

Kitchen, D. B., Hirata, F., Westbrook J. D., Levy, R. M., & Yarmush, M. (1990) *J. Comput. Chem. 11*, 1169–1180.

Kossiakoff, A. A., Simtchak, M. D., Shpungin, J., & Presta, L. G. (1992) *Proteins: Struct., Funct., Genet. 12*, 223–236.

Kundrot, C. E., & Richards, F. M. (1987) *J. Mol. Biol. 193*, 157–170.

Kundrot, C. E., & Richards, F. M. (1988) *J. Mol. Biol. 200*, 401–410.

Kundrot, C. E., Ponder, J. W., & Richards, F. M. (1991) *J. Comput. Chem. 12*, 402–409.

Levitt, M., & Sharon, R. (1988) *Proc. Natl. Acad. Sci. U.S.A. 85*, 7557–7561.

Li, T., Hook, J. W., Drickamer, H. G., & Weber, G. (1976) *Biochemistry 15*, 5571–5580.

Madura, J., & Pettitt, M. (1988) *Mol. Phys. 64*, 325–331.

McCammon, J. A., & Karplus, M. (1979) *Proc. Natl. Acad. Sci. U.S.A. 76*, 3585–3589.

McCammon, J. A. & Harvey, S. C. (1988) *Dynamics of Proteins and Nucleic Acids*, Cambridge University Press, Cambridge, England.

Millers, F. J., LoSurdo, A., & Chin, C. (1978) *J. Phys. Chem. 82*, 784–792.

Otting, G., Piepinsh, E., & Wuthrich, K. (1991) *Science 254*, 974–980.

Richards, F. M. (1977) *Annu. Rev. Biophys. Bioeng. 13*, 331–363.

Sarvazyan, A. (1991) *Annu. Rev. Biophys. Biophys. Chem. 20*, 321–342.

Sarvazyan, A. P., Kharakoz, D. P., & Buckin, V. A. (1992) *CRC Crit. Rev. Biochem.* (submitted for publication).

Samarasinghe, S., Campbell, D. M., Jonas, A., & Jonas, J. (1992) *Biochemistry* (in press).

Teeter, M. (1991) *Annu. Rev. Biophys. Biophys. Chem. 20*, 577–600.

Van Eldik, R., & Jonas, J., Eds. (1987) *High Pressure Chemistry and Biochemistry*, NATO ASI Series 197, D. Reidel, Dordrecht, The Netherlands.

Visser, A. J. W. G., Li, T. M., Drickamer, H. G., & Weber, G. (1977) *Biochemistry 16*, 4879–4881.

Wagner, G. (1980) *FEBS Lett. 112*, 280–284.

Weber, G., & Drickamer, H. G. (1983) *Q. Rev. Biophys. 16*, 89–112.

Weiner, S. J., Kollman, P. A., Nguyen, D. T., & Case, D. (1986) *J. Comput. Chem. 7*, 230–239.

Wlodawer, A., Deisenhofer, J., & Huber, R. (1986) *J. Mol. Biol. 193*, 145–156.

Wong, P. T. T. (1988) *Biochim. Biophys. Acta 956*, 1–9.

Wong, P. T. T. (1991) *Can. J. Chem. 69*, 1699–704.

Zipp, A., & Kauzmann, W. (1976) *Biochemistry 12*, 4217–4228.